Article

Not peer-reviewed version

Links between Land Cover and in-Water Optical Properties in Four Optically Contrasting Swedish Bays

Susanne Kratzer * and Martin Allart

Posted Date: 20 September 2023

doi: 10.20944/preprints202309.1382.v1

Keywords: Land Use and Land Cover (LULC); in-water optical properties; bio-optics; suspended particulate matter; coloured dissolved organic matter; chlorophyll-a; catchment area; water discharge; land-sea interactions.

Article

Links between Land Cover and in-Water Optical Properties in Four Optically Contrasting Swedish Bays

Susanne Kratzer [1,*] and Martin Allart [1,2]

[1] Department of Ecology, Environment and Plant Sciences (DEEP), Stockholm University, 106 91 Stockholm, Sweden

[2] National Institute of Applied Sciences (INSA), 20 Av. Albert Einstein, 69100 Villeurbanne, France

* Correspondence: Susanne.Kratzer@su.se

Abstract: The optical complexity of coastal waters is mostly caused by the water discharged from land carrying optical components (such as dissolved and particulate matter) into coastal bays and estuaries, and increasing the attenuation of light. This paper aims to investigate the links between in-water optical properties in four Swedish bays (from the northern Baltic proper up to the Bothnian bay) and the land use and land cover (LULC) in the respective catchment of each bay. The optical properties were measured in situ over the last two decades by various research and monitoring groups while the LULC in each bay was classified using the Copernicus Land Monitoring Service based on Landsat 8 and Sentinel-3 data. The absorption coefficient of coloured dissolve organic matter (CDOM) at 440 nm, *a*CDOM (440), and its spectral slope factor, *S*CDOM, were mostly correlated to natural land cover classes (Wetland, Meadow) acting as sources of CDOM, while Agricultural and Urban classes seem to act as sinks. The Agricultural class was also found to be a sink for suspended particulate organic matter (SPOM) whilst Coniferous and Mixed Forests as well as Meadows acted as a sources. SPOM seems to mostly originate from *Natural* classes, possibly due to the release of pollen and other organic matter. Overall, the methods applied here allow for a better understanding of effects of land used and land cover on the bio-optical properties, and thus coastal water quality, on a macroscopic scale.

Keywords: Land Use and Land Cover (LULC); in-water optical properties; bio-optics; suspended particulate matter; coloured dissolved organic matter; chlorophyll-a; catchment area; water discharge; land-sea interactions

1. Introduction

Seen from Space, or from a plane, coastal waters are usually not blue but often yellow or brownish, or even green or red during certain phytoplankton blooms. The yellow-brown shades are due to one of the main optical components found in natural waters: CDOM, also referred to as "yellow substance". It consist of humic and fulvic substances [1] which originate mostly from decomposing plant material and have a complex chemical nature, consisting mostly of diverse polymers with aromatic rings and long-chains of alkyls [2]. Humic substances are derived from the decomposition of plants and are ultimately drained into coasts by rivers and by runoff from land [1]. CDOM has a high absorption in the UV-blue spectrum which decreases with increasing wavelength towards the red in a logarithmic manner. Thus, CDOM appears yellow. Besides particle scatter, CDOM absorption is one of the key inherent optical properties (IOP's) of seawater. Preisendorfer [3] defined the IOP's as those optical properties that are independent of the radiance distribution, while apparent optical properties (AOP's) – such as diffuse attenuation or Secchi depth - are also influenced by the sun angle and thus the radiance distribution.

Carder *et al.* [4] studied the nature of CDOM in the Gulf of Mexico and determined that they could either be of a more humic character (i.e. larger molecules and a slope factor S_{CDOM} closer to -0.0011) when related to bogs, or a more fulvic character (i.e. smaller, i.e. more degraded molecules, and a slope factor closer to -0.0022). The Baltic Sea is rich in dissolved organic carbon (DOC), the

 doi:10.20944/preprints202309.1382.v1

light-absorbing fraction of which is referred to as CDOM. Harvey et al. [5] found that the slope factor S_{CDOM} varied over the year, both in the Gulf of Bothnia (with a high terrestrial input) as well as in the NW Baltic proper (with a relatively low terrestrial input.

CDOM absorption is particularly high in the Baltic Sea compared to other seas and oceans around the world [1]. In the Baltic Sea CDOM is the main optical constituent determining the light attenuation, especially in coastal areas [6,7]. Another important optical component in coastal waters is SPM, consisting of solid particles made up by both inorganic sediments (sand and silt), by organic material (usually in minor proportions) and by phytoplankton. The absorption characteristics of SPM are usually difficult to measure because it also scatters light, especially its inorganic fraction [8,9]. Light scattering by particles depends on particle composition, size and shape as well as the refraction index of the particles [10]. Because of their high water fraction, phytoplankton have a relatively low refractive index of 1.02-1.07 while inorganic particles have a high refractive index ranging from 1.1-1.26 [11–14]. Inorganic SPM is usually found in coastal areas and indicates coastal influence [7,15].

SPM is often found in large proportions in coastal waters and may indicate physical forcing such as wind-wave action, eddies and tidal currents, causing the resuspension of sediments derived from discharge of particle-laden rivers [16,17]. The absorption properties of non-algal organic SPM are similar to those of CDOM but with a different spectral slope [18].

The study by Le et al. [19] evaluated the effect of LULC derived from remote sensing data on the inherent optical properties of several estuaries in the northern Gulf of Mexico. Initially, the authors derived eight main classes: *Urban, Agriculture, Evergreen Forest, Deciduous forest, Water, Wetland, Range Land* and *Barren Land*. Next, they compiled the *Urban* and *Agriculture* class into a *'Developed'*, and *Evergreen Forest* and *Wetlands* into a *'Natural'* class. They could then show that there were significant correlation between the optical properties and the ratio of *Developed* to *Natural* LULC classification across 6 bays.

The aim of this paper is to describe the optical characteristics of four Swedish bays in relation to the LULC characteristics of the respective catchment of each bay. First, the catchment area of each bay is defined based on the hydrology. The LULC characteristics are then derived from remote sensing data, and are further analyzed using an Open Source Geographic Information System (GIS). Subsequently, the relationship between LULC cover and optical properties is evaluated via correlation analysis. One of our main hypotheses is that catchments with a relative large percentage of bogs and a larger extent of natural land cover are characterized by higher CDOM absorption.

The objectives of this study can be summarized in the following way: Firstly, we will assess the nature of the CDOM absorption at 440 nm and the CDOM slope factor of each bay in relation to the proportion of different natural land categories. Secondly, we will evaluate if different land cover categories may have an effect on the SPM load, or on the nature of the SPM found in the four coastal bays. Thirdly, we will investigate if LULC has an effect on the levels of chlorophyll-a (Chl-a) concentration found in the bays, and, finally, we will investigate if there are any relationships between LULC cover and bio-optical water quality that are specific for Scandinavia and the high latitudes.

2. Materials and Methods

2.1. Site descriptions

For the analysis, we selected four Swedish bays where measurement transects of optical in-water variables (e.g. Chl-a, CDOM, SPM and turbidity) were performed over the last two decades by the Marine Remote Sensing Group (MRSG) and the pelagic Monitoring Group (MG) at DEEP, Stockholm University, and also during 2018 through a collaboration between MRSG and the monitoring group from Umeå Marine Sciences (UMF), Umeå University.

Figure 1) indicates the two zones of this study: Zone 1 comprising the northern Baltic proper and the Åland Sea, and Zone II in the Bothnian Bay. Optical measurements were performed along transects through the different bays (see section 2.2 below). A numerical analysis of the land cover in

Preprints (www.preprints.org) | NOT PEER-REVIEWED | Posted: 20 September 2023 doi:10.20944/preprints202309.1382.v1

the catchments surrounding those bays was carried out using the Geographic Information System (GIS) software, QGIS. A catchment is here defined as the natural drainage area, i.e. a zone where rainfall flows into streams, rivers, lakes and ground waters, and eventually ends up in certain water bodies (basins) or bays. Section aims at describing the selected bays and the main surrounding elements (both natural and artificial) that affect these coastal water bodies while section 2.1.2 is dedicated to the description of catchments and rivers related to these bays.

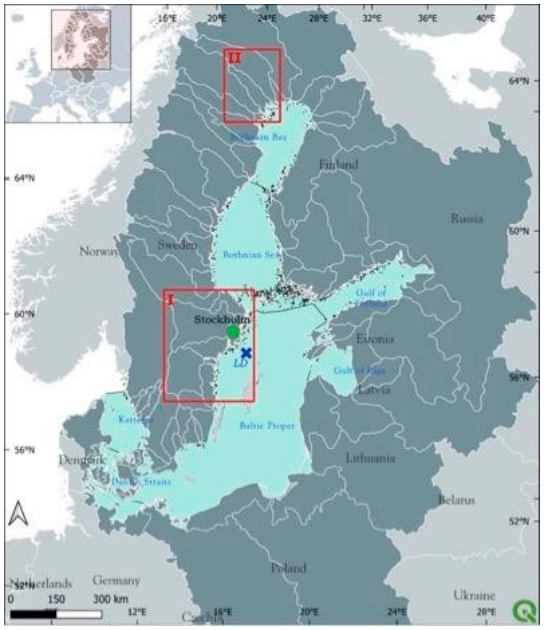

Figure 1. Overview of the Baltic Sea and its location within Europe. Zone I and II are areas of interest for the study. Source: Baltic Sea catchment area and HELCOM Sub-basins 2018 [20] Country boundaries: Natural Earth [21], European coastline shapefile: EEA [22], SMHI's sub-basin division (havs-områden_SVAR_2016 [23]).

2.1.1. Description of each site (bay)

Bråviken bay (Figure 2a) is a large east-west facing bay. Its topography is particularly shallow with a depth gradient from its southern bank (mean depth: 10 m) to its northern bank (mean depth: 40 m). The Swedish Water Archive divides the bay into 5 sub-basins: Pampusfjärden (A), Inner Bråviken (B), Mid-Bråviken (C), Outer Bråviken (D), Bråviken's coastal waters (E). Several sampling stations (BR1-BR9) of the MRSG (SU) are located along a salinity gradient from the inner bay towards (A) the open sea (E). Many industrial sites are established in the bay and several pulp industry premises are located on the shores of Pampusfjärden and the bay also hosts Europe's largest grain facility port for export which leads to a lot of ship and boat traffic inside the bay.

Himmerfjärden bay (Fig 2b), is a narrow, elongated bay facing from north to south and it is deeper than Bråviken (40 m mean depth). In the inner bay, there is a sewage treatment plant, which is the third largest in Stockholm County. Himmerfjärden bay consists of several basins that are separated by sills, and is also fragmented by many islands of various size which makes the water circulations more complex than in Bråviken. The water basins in HFj are called Näslandfjärden (W), Himmerfjärden (X), Svärdsfjärden (Y) and Krabbfjärden (Z). Himmerfjärden bay surrounds a central island called Mörkö which hosts recreational sites and natural reserves as well as summer houses. There is a salinity gradient from the inner bay (W) out into the open sea (X), as well as a gradient of optical properties **[7].** The optical transects considered in this study starts at station H6 Näslandfjärden (W) going out to H2 in Svärdsfjärden (Y). An extra station B1 is located in Krabbfjärden in the SW of the island Askö (which is a nature reserve and home of Askö Laboratory, sustained by Stockholm University). Even though B1 is shielded by the island and not part of the chosen optical transect, it has shown to have similar optical characteristics as station H2 just inside

Preprints (www.preprints.org) | NOT PEER-REVIEWED | Posted: 20 September 2023 doi:10.20944/preprints202309.1382.v1

Hfj bay **[7]**. This is why the optical variable of station B1 and H2 were combined and averaged in the analysis detailed below.

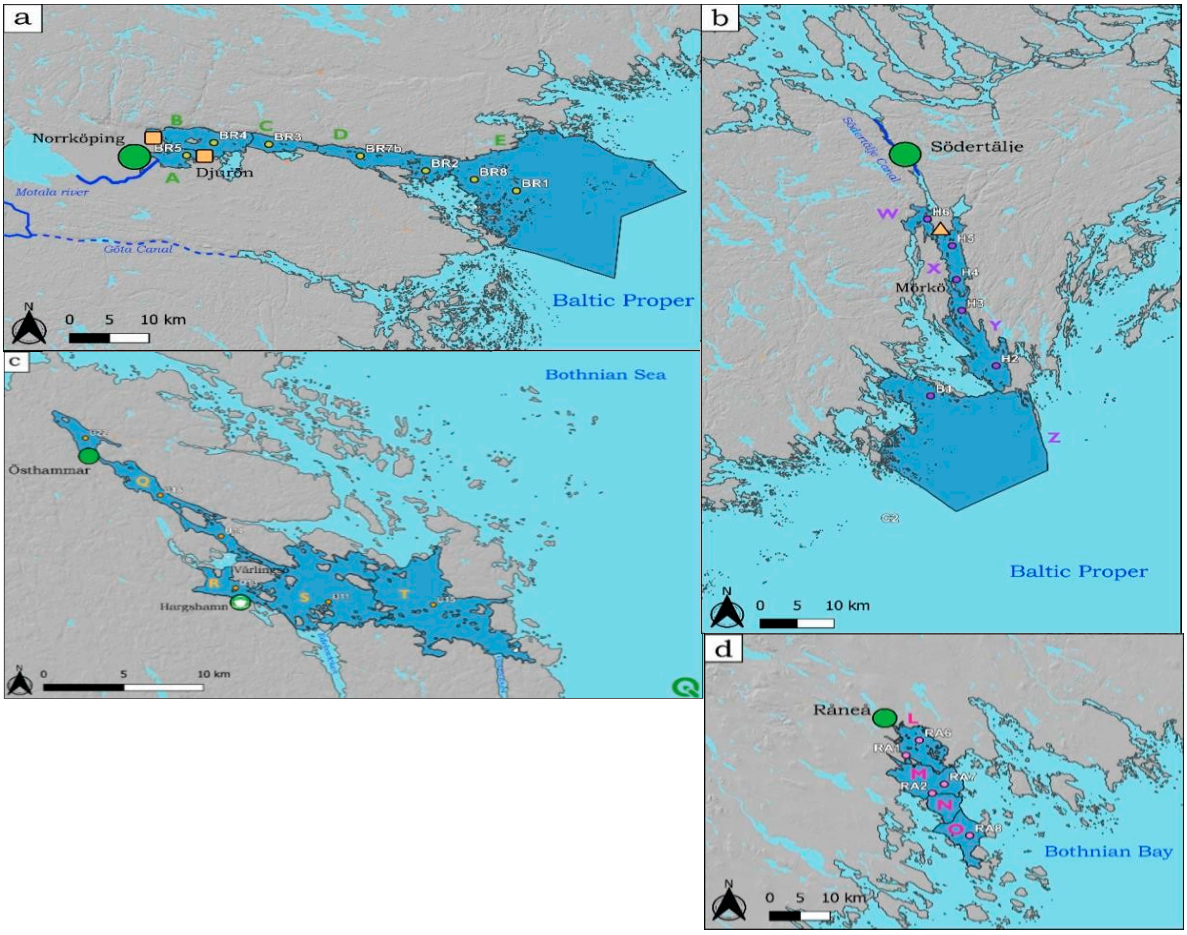

Figure 2. The four Swedish bays, their sub-basins and sampling stations. Zone I: Bråviken (a), Himmerfjärden (b), Östhammar (c). Zone II: Råneå (d). Map generated in QGIS using predefined shapefiles (European coastline shapefile [22]), SMHI's sub-basin division (havs-områden_SVAR_2016 [23]). Recurrence layer – Global Surface Water, Surface elevation – Copernicus EU-DEM- v1.1; Sentinel Hub [24]). .

Östhammar bay (Fig 2c) is very shallow and lies in the Åland Sea which is adjacent to the most southern part of the Bothnian Sea. It can be regarded as a bay even though its shape is more complex than those of the other bays of zone I. Its main branch stretches from SW to NE. Its sub-basins are: Östhammarfjärden (Q), Hargsviken (R), Galtfjärden (S) and Singöfjärden (T). The transect of measurement originates at station U22 towards the outermost station U15, along an increasing salinity gradient. Station U18, U14, U13 and U11 lie in between. At the junction of the sub-basins Q, R and S there is a large island called Värlingsö. The water flows from the inner Östhammar bay (Q) into R where the municipality of Hargshamn is located with its large, industrial port. This part of the bay is deeper than the passage flowing from Q to S-basin, which allows the passage of cargo boats. The water flow is thus more important the R-S than in Q-S passage. The second inlet branch of the bay is called Edeboviken, where station U12 is usually sampled by the pelagic Monitoring Group (MG) from Stockholm University, but it was rejected from the analysis here because its optical properties have shown to be very different from U13. The presence of Väddöviken bay at the end of the transect might also influence the optical characteristics of the last sampling station U15. The remainder of the bay, i.e. denoted basins S and T (Figure 2c), are fragmented by many islands which makes the circulation of water rather complex.

Råneå bay (Figure 2d) is located in the western Gulf of Bothnia (zone II, Figure 1), where the waters in the surface layers are frozen during winter, and usually have a very high content of CDOM

 doi:10.20944/preprints202309.1382.v1

from riverine sources **[26].** The coastal waters are characterized by a very strong coastal influence both after the ice thawing in spring and all during summer. The sampling station RA1, RA2, RA6, RA7 and RA8 are located in 4 sub-basins, stretching from the inner bay towards the outer bay: Råne fjärden (L), Gussöfjärden (M), Tistersöfjärden (N) and Fjusköfjärden (O).

2.1.2. Selection of catchments and description of the hydrology

The catchments surrounding the bays were selected based on the '*Water Web*' of the Swedish Meteorological and Hydrological Institute (SMHI), that can be used to assess the Current Hydrological Status in a certain catchment area **[25],** as mentioned above, a catchment is defined as an area from which rain and river water flows into other downstream waterbodies. We initially selected both the greater catchment zone for each bay (shapefile haro_y_2016_3) as well as the sub-catchments directly surrounding the bays (shapefile aro_y_2016_3). Eventually, these areas were merged as to constitute the greater catchment zone of interest for each of the 4 bays, respectively (**Figure 3a and 3b**). The average discharge value for each month over the period 1991-2021 was derived for each discharge basin and summarized in an Excel spreadsheet. The size of the catchments varied from only 993 km^2 for Östhammar bay to 23 368 km^2 for Himmerfjärden bay. The freshwater discharge value also varied considerably with the lowest value for Östhammar bay, about 4 $m^3\ s^{-1}$ on a yearly average (see **Supplementary Figures S3),** and the highest value for Bråviken of about 65 m3 s^{-1} on a yearly average. One can explain such big differences by the size of the catchment, and also the presence of the main Swedish rivers.

In Bråviken for instance, the Motala river (**Figure 3a**) is connected to Lake Vättern and leads into Pampusfjärden (area A, **Figure 2a**) passing through Motala, Linköping, and eventually Norrköping. Lake Vättern, with a total surface area of 1 912 km^2 is the second largest lake of Sweden and the sixth largest lake in Europe. It thus generates a considerable freshwater flow of about 50 m^3s^{-1} at its source in Motala, gathering even more discharge water on its way to Norrköping where the water flow reaches about 100 m^3s^{-1} in winter and spring, and around 50 m^3s^{-1} in summer and autumn (**Supplementary fig. S3b**). Vättern also exhibits downstream connections with the Göta Canal, while one section flows down into Lake Vänern and another into the Baltic Sea (Figure 3), but the water flows are negligible when compared to Motala river (less than 1 m^3s^{-1}). The Bråviken catchment is composed of two parts - its greater catchment (light green) and its surrounding catchment (dark green).

Himmerfjärden bay originates by approximately 50% from the streams of its surrounding catchment (dark purple) and ca. 50% from its greater catchment (light purple), collecting all the discharge water into Lake Mälaren (Figure 3a). Unlike the greater catchment of Bråviken, it is not connected by a natural river but with the Södertälje Canal, named after the town it passes through. This canal is regulated by locks and has a very low and almost constant flow of freshwater of about 5 m^3s^{-1}. During events of floods and heavy rainfall, the locks can be opened up to alleviate the flooding risk in Stockholm City and the discharge jumps then suddenly up to 100 m^3s^{-1}, but these kinds of events are quite rare and did not occur during any field campaign considered in this study. The yearly average of freshwater discharge is estimated to be 8 m^3s^{-1} (see **Supplementary fig. S3a**). The Östhammar bay receives its waters from various streams and small rivers. The catchment includes many small lakes and minor bogs which explains why the water outflow is only about 4 m^3s^{-1} on a yearly average. The value even decreases to a minimum value of 0.5 m^3s^{-1} during summer because its small streams evaporate to a large extent before reaching the coast (see **Supplementary fig. S3a).**

Preprints (www.preprints.org) | NOT PEER-REVIEWED | Posted: 20 September 2023 doi:10.20944/preprints202309.1382.v1

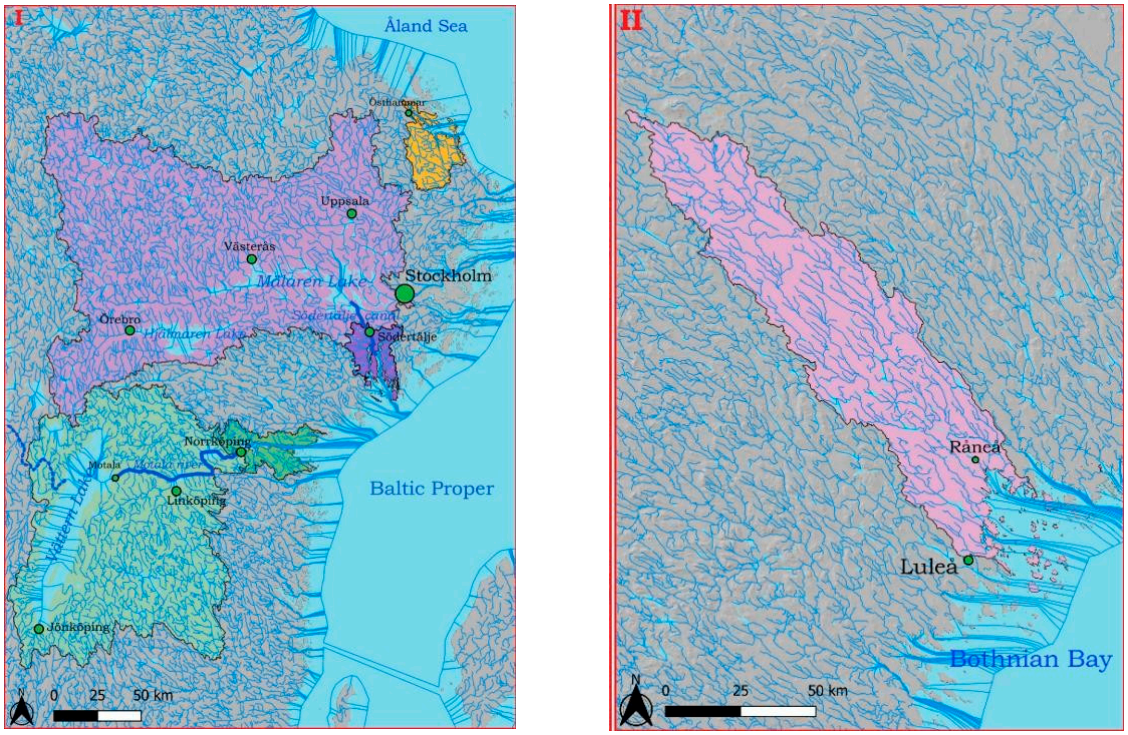

(**a**) (**b**)

Figure 3. a. Catchments of zone I. Light and dark green: Bråviken bay. Light and dark purple: Himmerfjärden bay. Orange: Östhammar bay. Maps generated in QGIS using predefined shapefiles (European coastline shapefile **[22]**), Recurrence layer – Global Surface Water, Surface elevation – Copernicus EU-DEM- v1.1; Sentinel Hub **[24]**), Water course network **[25]. Figure 3b.** The Råneå estuary is located in zone II in Swedish Lapland (see also Fig 1). Its landscape is highly influenced by a myriad of various streams, converging into the Råneå river. The shape of the discharge variation curve along the year is remarkably different from the catchments of zone I. A major peak in mid-May can be observed every year induced by the thawing of sea ice and snow. It gives rise to huge discharge of about 320 m^3s^{-1} at its maximum (see **Supplementary Fig. S3b).** The inflow of freshwater decreases to about 50 m^3s^{-1} during May, and then progressively further down to ca. 20 m^3s^{-1} during the winter months. .

2.2. Optical transects

The MRSG performed two satellite validation campaigns in Bråviken bay on board R/V Electra during 1-2 July 2021 and 28-29 of April 2022. Optical measurements were taken along transects with a salinity gradient (Figure 2a) from the inner bay (A) out to the open Baltic Sea (E). The data from the field campaigns in 2021 and 2022 was merged with other transects from past expeditions performed over the last 15 years in the four bays (**Table 1**). It must be noted that the MRSG has trained the pelagic monitoring groups at SU and UU over the last two decades on how to perform optical measurements (e.g. CDOM, SPM and turbidity) and the groups share their optical protocols and also intercompare their methods **[27]**). Table 1 provides a summary of the measurements performed, including dates, operating group and number of samples gathered. Altogether n = 116 stations were sampled for this study, including measurements of Chl-a, SPM, SPIM, SPOM concentrations, turbidity (t), Secchi Depth (SD), CDOM absorption, a_{CDOM} and the CDOM slope factor, S_{CDOM}. The largest collection of data comes from the Himmerfjärden area.

2.2.1. Water sampling and measurement protocols

Note that the procedures below follow the Optical Measurement Protocols of the Marine Remote Sensing Group. During the field work, the samples were gathered 20-30 cm below the water surface with a sturdy sampling bucket with a pip. The bucket was rinsed twice with sea water

Preprints (www.preprints.org) | NOT PEER-REVIEWED | Posted: 20 September 2023 doi:10.20944/preprints202309.1382.v1

before sampling as to avoid contamination. The sampling bottles were also rinsed twice with sea water and then filled with sea water from the bucket. The same standard protocol was applied for all other field campaigns by the MRSG but other laboratories sometimes have slightly different protocols. Nonetheless, intercomparison workshops are held regularly to make sure that the measurements between groups are comparable **[27].**

2.2.1.1. SPM, SPIM and SPOM measurements

Depending on the Secchi depth reading, 1- 2 L of sea water were sampled for SPM measurements. The measurements were performed using the gravimetric method developed by Strickland and Parsons **[28].** This method consists of filtering a certain quantity of natural water through microfibers glass filters (GF/F filters) of 47 mm diameter and with a nominal pore size of 0.7 µm. Before filtration, the filters were pre-rinsed with ultra-pure water (UPW), combusted and pre-weighed (tare weight) with a high-precision scale (Satorius MP3 microbalance – ± 1 µg). Note that every sampling bottle was gently mixed before filtration (for the resuspension of particles). All filters were rinsed at the end of the filtering process with 100 mL UPW for removal of salt residuals. After filtration each filter was placed in a numbered (by etching), clean square aluminium foil (10 x10 cm). Then, the filters were dried for at least 4 hours in 60 ºC (alternatively overnight). The filters were subsequently stored in a desiccator in order to keep them dry until weighing. The dry weight of SPM was derived by subtracting the tare weight from the dry weight. In order to derive SPIM, the filters were combusted for 5 hours at 480 °C, and were weighed again. The organic fraction was then derived from the weight difference between the total SPM (dry weight) and the SPIM (combusted weight), assuming all organic matter has been combusted. The handling of the filters sometimes leads to the loss of filter bits. Therefore, triplicate filters were taken for every station as quality control of the measurements. Outliers were removed if the standard deviation was more than 20%. For every field campaign between 5 and 10 blank filters were processed in the same way except that ultra-pure water (UPW) was used (0.5 L) instead of sea water, and their average weight was then used to correct for handling errors. The standard error of the method is 10% **[29].** In the Bothnian bay, the rinsing with UPW was sometimes omitted by mistake by the local monitoring group, and during the data quality control (i.e. comparison against the measured turbidity values), the samples were found to be invalid and therefore had to be omitted.

Table 1. Overview table of stations (n) sampled in the 4 areas of investigation. The full data set can be found in Table S2. .

	Bråviken	Himmerfjärden		Bay Östhammar		Råneå	
Apr 2022	n=5 (MRSG)	**Apr2018**	n=4 (MRSG) SPM, SPIM, SPOM missing	**Aug 2021**	n=4 (MG) SPM, SPIM, SPOM missing	**Jul 2018**	n=4 (MRSG & MG UMF)SPM, SPIM, SPOM not valid
Jul 2021	n=6 (MRSG) SPM, SPIM, SPOM missing	**Aug2017**	n=5 (MG)	**Jul 2021**	n=4 (MG) SPM, SPIM, SPOM missing	**Jun 2018**	n=4 (MRSG & UMF) SPM, SPIM, SPOM not valid
Apr 2018	n=8 (MRSG) *Sc*DOM missing	**Jul 2017**	n=4 (MRSG)	**Aug 2020**	n=4 (MG) SPM, SPIM, SPOM missing	**May 2018**	n=4 (MRSG & UMF) SPM, SPIM, SPOM not valid
Aug 2013	n=2 (MG) turbidity, *Sc*DOM missing	**May2012**	n=4 (MRSG)	**Jul 2020**	n=4 (MG) SPM, SPIM, SPOM missing		
Jul 2013	n=2 (MG) turbidity, *Sc*DOM missing	**Apr2012**	n=3 (MRSG)	**Aug 2019**	n=4 (MG) SPM, SPIM, SPOM missing		
Jun 2013	n=2 (MG) turbidity, *Sc*DOM missing	**Aug2010**	n=8 (MRSG)	**Jul 2019**	n=4 (MG) *Sc*DOM , *a*CDOM, SPM, SPIM, SPOM missing		
Aug 2012	n=2 (MG) *Sc*DOM missing	**Jul 2007**	n=13 (MRSG)	**Aug 2010**	n=4 (MG) turbidity missing		

Jun 2012	n=2 (MG) S_CDOM missing			**Jul 2010**	n=6 (MG) turbidity missing		
Total stations sampled: **n = 29**		Total stations sampled: **n = 41**		Total stations sampled: **n = 34**		Total stations sampled: **n = 12**	

2.2.1.2. Turbidity measurements

Turbidity was measured during field campaigns with a portable turbidity meter (*Hach Lang 2100Qis*). The calibration of the device is done using standard formazin solutions of known turbidity (10, 20, 100, 800 FNU). Formazin Nephelometric Unit (FNU) is a unit equivalent to NTU but is measured in the near infrared (NIR) rather than using white light. The standard calibration solutions are provided by the manufacturer. Before performing a measurement, one gently mixes a sample **[16]**. It is important to wait for 10 s before starting the measurement in order to get rid of air bubbles that could cause extra scattering, and thus wrongly increase the turbidity value. Each turbidity sample was measured 5 times and the values were averaged and corrected for the average turbidity value of ultrapure water (UPW) which was also measured 5 times.

2.2.1.3. CDOM Measurements

The CDOM samples were collected in 250 mL amber glass bottles and the samples were filtered through 0.22 µm membrane filters using glass filtration unit fitted with a metal mesh to avoid clogging of the filtering unit. The filtrate was then transferred into 100 mL amber glass bottles and stored in a fridge at 4 Cº for up to 3 months. The absorption spectra of CDOM was measured by scanning the sample in a Shimadzu UVPV-2401 dual beam spectrophotometer (Shimadzu Corporation, Kyoto, Japan). Before scanning, the samples were removed from the fridge and allowed to reach room temperature (overnight). The absorption spectrum was measured in the range from 350 to 800 nm in cylindrical quartz cuvettes (10 cm). First, a baseline was performed, using both cuvettes filled with UPW. The cuvette in the back was then used as a reference (filled with UPW). The front cuvette was then filled with the sample water and scanned. A complete absorption spectrum was then obtained (in 1 nm steps). The value at 700 nm was used to correct for measuring errors and the spectral absorption coefficient for CDOM was derived from the following relation, according to Kirk **[1]:**

$$a_{CDOM}(\lambda) = \ln(10)\,\mathrm{OD}(\lambda)\mathrm{L}^{-1},\ [m^{-1}] \quad (1)$$

with OD(λ) being optical density, L being the optical path length of the cuvette in meter, here 0.1 m. Note that the OD is measured in logarithmic values (Ln10). The absorption at 440 nm, g_{440}, is thus derived per meter after log-transformation. The absorbance was first corrected for the reading at 700 nm and then converted to absorption; then the whole spectrum was log-transformed, providing a linear regression. Subsequently, the slope in the range of 350 to 500 nm was derived, which corresponds to the slope factor of CDOM, S_{CDOM}.

2.2.1.4. Chlorophyll-a measurements

0.2 - 0.5 L of sea water were filtered onto 25 mm diameter GF/F filters. Filtering was performed on board ship and the filters were flash-frozen in liquid nitrogen and stored for 2 weeks. Each sample was filtered and measured in triplicates. Before the spectral analysis, the samples were placed in 5 mL of 90% acetone solution and sonicated for 30 s for destruction of the cell walls and extraction in acetone. The samples were then centrifuged for 10 min at 3000 rpm so that all particles could settle in the bottom of the polypropylene test tube and thus avoid the effect of scattering on the absorption spectrum. After 30 minutes of extraction, the samples were transferred into 1 cm quartz cuvettes and scanned against 90 % acetone (350-850 nm) in a Shimadzu UVPC-2401 dual beam spectrophotometer. The spectra were then processed in Excel with the algorithms and coefficients provided by Strickland and Parsons **[30]** in order to derive the *Chl-a* concentration in µgL^{-1}. This method has shown to be within 10% error during an inter-calibration performed by the ESA MERIS Validation Team **[31]** and within 2-10% when compared to the Swedish monitoring groups **[27].**

Preprints (www.preprints.org) | NOT PEER-REVIEWED | Posted: 20 September 2023 doi:10.20944/preprints202309.1382.v1

2.3. Land Use and Land Cover analysis

The land Use and Land Cover (LULC) of each bay was analysed in QGIS (version 3.26.2 'Buenos Aires'), an open-source Geographic Information System (GIS). Data from two sources were used, firstly shapefiles from the Swedish Hydrological Meteorological Institute (SMHI), which provided the polygons shapefiles of the Swedish catchments (Haro) and sub watersheds (aro) around the different bays of the study using SVAR version 2016_3 **[23];** maps of the different catchment areas are shown in Figure 3.

The catchment area selection was not trivial and was performed with regards to hydrological data from the SMHI and freshwater discharge values **[25]**. Secondly, we used CORINE Land Cover 2018 (CLC2018) database derived from Sentinel-2 and Landsat-8 satellites images **[24]**.

This dataset provided initially 44 land cover categories (see **Supplementary Table S1**) which were further aggregated into 10 classes for this study (Figure 4). The following operations were performed to process the data in QGIS:

- Reprojection of CORINE into the same geographical projection as for the Catchment shapefile EPSG3006 SWEREF99 TM used by the Swedish Meteorological and Hydrological Institute, SMHI [23].
- Fixing geometries of CORINE data via the vector operation "fix geometries"
- Reduced the number of Level 1 attributes from 44 to 10 categories (so called code_18).
- Aggregating the original 44 to 10 polygons of the same Level 1 class.
- Intersection of the dissolved LULC polygons with the catchment boundaries to get rid of information outside the areas of interests.
- Eventually, computation of percentage area per category of Level 1.

Figure 4. Legend for the final 10 aggregated LULC classes.

All 11 urban classes from the original 44 classes were gathered under the class *Urban*. All arable land, permanent crops and heterogeneous agricultural areas (consisting of 10 classes) were aggregate into *Agriculture*. The class *Pastures* was left as designated in CORINE. It may differ from the *Agriculture* class due to the manure from cattle, and also from the class *Meadow* which refers to land that is covered by different natural grass types and bushes. All open spaces with little or no vegetation were assembled into one class: *Barren Land*. The four shrub classes aggregated into the *Meadow* class. All 5 wetlands classes were united into a *Wetland* class. Similarly, the 5 water subcategories into one *Water* class. *Deciduous forest*, *Coniferous forest* and *Mixed forest* were left unchanged.

2.4. Combining optical and LULC data

All data were collected and processed in Excel for further analysis. A first analysis was done in order to operate a data quality check. From the geographical coordinates of a given station the horizontal distance (in km) from an outlet was derived with the aim to make the transects within the 4 bays comparable. The outlet was chosen to be either a defined river mouth (cf. Östhammar and Råneå), or the innermost station usually sampled by the respective monitoring or research group

Preprints (www.preprints.org) | NOT PEER-REVIEWED | Posted: 20 September 2023 doi:10.20944/preprints202309.1382.v1

(e.g. station H5 and BR5 in Himmerfjärden and Bråviken). A new data sheet was then compiled for each optical parameter, and various plots were made to visualise the data, either season-wise or regardless of the time of the year. It allowed to identify outliers and observe variability between the bays as well as seasonal variability, and to choose which variable to focus on. Finally, the stations were aggregated based on their horizontal distance from the outlet. The optical properties in each transect were then averaged by taking the geographic middle stations. The mean horizontal distance from the outlet ranged from around 15 ± 5 km in the different areas. Any innermost or outermost station making the mean distance deviating from this range were rejected from the study in order to make the data sets comparable. This workflow is summarised in Figure 5.

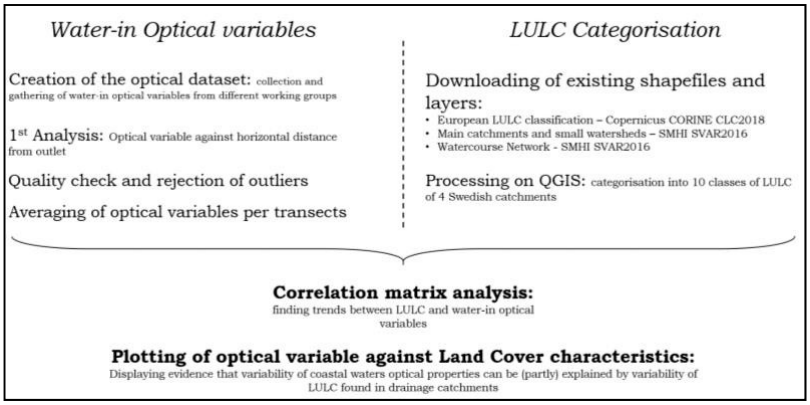

Figure 5. Workflow diagram of data processing method.

The respective optical variable was then averaged for every transect. It was eventually possible to plot an optical variable against a LULC information such as a percentage of a given land cover, or a ratio of several land covers. To better understand the contribution and influence of every LULC class on the optical variables, a correlation matrix was prepared. The correlations in the matrix were then tested using a significance test based on the p-value test with $\alpha = \mathbf{0.05}$.

Le et al. [19] observed in their study that groups of LULC categories should be assembled in order to relate them to optical properties on a macroscopic scale. They derived a *Natural* category (*Coniferous Forest* + *Wetland*) as well as a *Developed* category (*Urban* + *Agriculture*). Eventually, they inferred that the *Ratio Developed* / *Natural* category showed interesting results when comparing to the optical properties of various estuaries in their study. As a first step, such group categories and ratios were also derived and tested for this study but were also adapted with regards to our correlation matrix and typical trends observed in Swedish bays (see results of the correlation analyses and tend analysis below). The natural class used here, denoted *Natural**, thus was merged to include *Coniferous Forest* + *Wetland* + *Meadows* while the developed class, denoted *Developed**, included *Urban* + *Agriculture* + *Pastures* (although the latter was so small in % area that it did not show any effect on the results, see below). Finally, the ratio of *Developed** over *Natural** was denoted *Ratio**. Next, the correlation matrix was used to evaluate the link between CDOM, LULC and Discharge. Correlations were applied between optical properties and the final LULC categories as well as the grouped categories *Natural**, *Developed** and *Ratio** as defined above, and also between optical properties and the discharge values derived for the different bays from the Current Hydrological Status on the SMHI Water Web [25].

3. Results

3.1. Variability of LULC in the catchments

Figure 6 shows an example of LULC map obtained in the surrounding catchment of Himmerfjärden bay. The LULC classification for the other three bays can be found in the supplementary data (**Supplementary Figures S2a-S2c**).

Preprints (www.preprints.org) | NOT PEER-REVIEWED | Posted: 20 September 2023 doi:10.20944/preprints202309.1382.v1

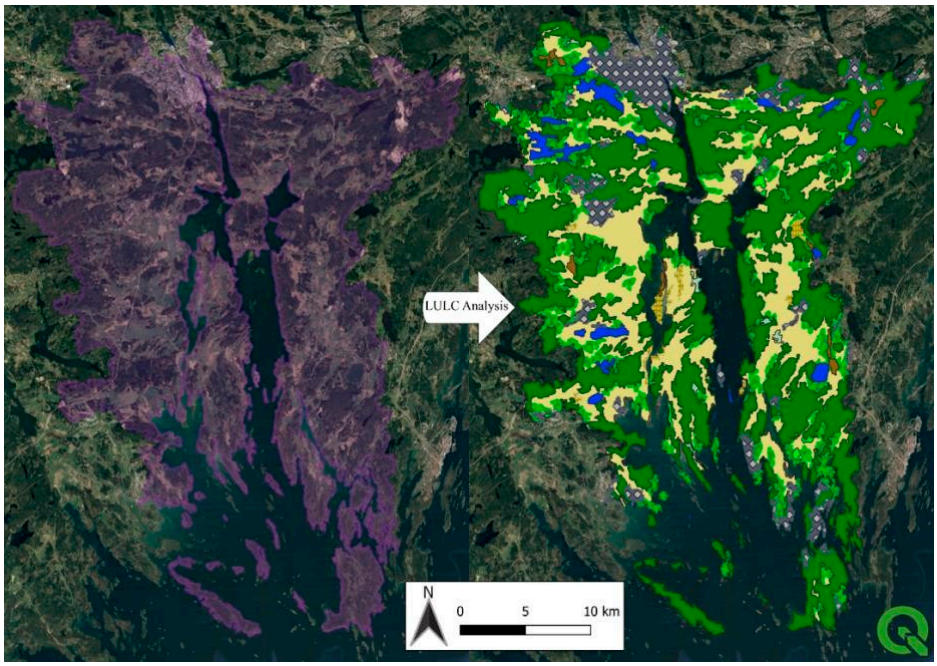

Figure 6. Map of the Himmerfjärden catchment before and after LULC analysis. Processed in QGIS using predefined shapefiles: main catchment areas (huvudavrinningsområden) - *SVAR2016_3* **[25],** *Land Cover* – Copernicus Land Monitoring Service (**[25];** Google Satellite. .

The results of the LULC classification for all four bays are presented in **table 2**. For each bay, the three major classes in percentage area are represented in bold characters. Bråviken (Br) and Himmerfjärden (Hfj) bays exhibit quite similar land cover profiles, except that Hfj is more artificially developed due to its slightly more important *Agriculture* and *Urban* classes (**Supplementary figures S2(a)-2(b))**. The Råneå estuary stands out with a much more *Natural* profile (**Supplementary figure S2c**). In this part of Swedish Lapland, the flora is not only dominated by *Coniferous forest* but also by vast *Meadows* (13.2%) and *Wetlands* (19.1%). Östhammar, located slightly to the North of Stockholm archipelago, displays an intermediate profile between that of Råneå, Himmerfjärden bay and Bråviken bay. On the one hand, *Agriculture* (11.3%) is the third most important class, but to a lesser extent than for Bråviken bay (20.0%) or Himmerfjärden bay (23.2%). On the other hand, its *Forest* coverage is more similar to that of Råneå bay.

Table 2 also shows that the leading LULC category in each catchment area is the category *Coniferous Forest*. This is very typical for Swedish forests which are dominated by Spruce and Pine which together make up about 80% of tree coverage **[32],** see **Supplementary Figure S1**). Overall, agriculture was the second most important land cover type, apart from the more pristine area Råneå in the north-western Bothnian Bay. Furthermore, mixed forest made up 4.3 % to 14.3% across all catchments, while the category *Water* was also important in the catchments of Bråviken (18.4%) and Himmerfjärden (10.6%) due to the influence of Lake Vättern (Bråviken) and the combined influence from Mälaren and Hjälmaren (Himmerfjärden).

Preprints (www.preprints.org) | NOT PEER-REVIEWED | Posted: 20 September 2023 doi:10.20944/preprints202309.1382.v1

Table 2. The variability of LULC in the catchment areas of four Swedish bays. Values were obtained after processing of Copernicus CORINE_2018 data in QGIS. The main LULC classes are shown in bold. Classes for which the surface area was 0-3% across all bays were rejected from further analysis (marked in light grey) as they did not have a visual impact on the correlation analysis (see below),and therefore were assumed not to have a significant effect on the optical properties in the coastal bays. .

	Urban	*Agriculture*	*Coniferous Forest*	*Deciduous Forest*	*Mixed Forest*	*Meadow*	*Pasture*	*Wetland*	*Water*	*Barren land*
Bråviken (Br) n = 29 (16,40×10³ km²)	2.6%	**20.0%**	**47.3%**	2.6%	4.3%	2.5%	1.4%	1.0%	**18.4%**	0.0%
Himmerfjärden (Hfj) n = 41 (23.37×10³ km²)	4.4%	**23.2%**	**47.4%**	1.2%	6.5%	4.0%	0.7%	1.5%	**10.6%**	0.5%
Råneå (Rå) n = 34 (5.67×10³ km²)	0.3%	1.5%	**52.4%**	1.1%	8.6%	**13.2%**	0.2%	**19.1%**	3.8%	0.0%
Östhammar (Östh) n = 12 (993 km²)	2.9%	**11.3%**	**56.2%**	1.8%	**14.3%**	8.1%	1.1%	0.7%	3.7%	0.0%

3.1. Investigating the nature of CDOM due to LULC

Figure 7 displays CDOM absorption at 440 nm, $a_{CDOM}(440)$ against the distance from the outlet for each respective bay (data from all seasons included). The maximum CDOM values were found in Råneå (up to about 6 m^{-1}) during the transect in May 2018, which corresponds to the snow and ice thawing period. At that time of the year the average water catchment discharge, Q, is about 300 m^3s^{-1} (Supplementary Figure 3b). The results from the correlation analysis of LULC categories vs. a_{CDOM} and S_{CDOM}, respectively are shown in **table 3.**

Figure 8a shows the averaged value per transect and bay for a_{CDOM} for all times of year in relation to Ratio*(Dev/Nat) . The results show that Råneå bay has the most natural catchment with a Ratio*(Dev/Nat) of around 0.023, followed by Öshammar bay (0.235), Bråviken (0.47) and Himmerfjärden bays (0.535).

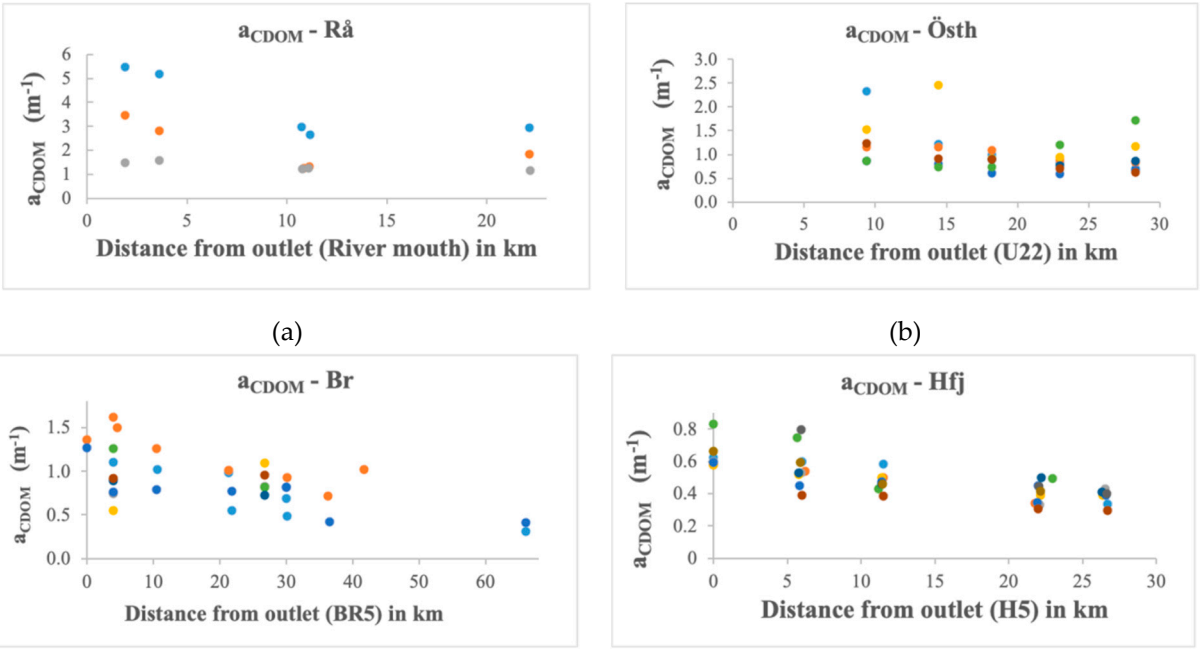

Figure 7. CDOM absorption at 440 nm, aCDOM, in four Swedish bays: (a) Råneå bay (Rå), (b) Östhammar bay (Östh), (c) Bråviken bay (Br) and (d) Himmerfärden bay (Hfj). Values are plotted

Preprints (www.preprints.org) | NOT PEER-REVIEWED | Posted: 20 September 2023 doi:10.20944/preprints202309.1382.v1

against horizontal distance from the outlet (in km). All transects were plotted within each bay regardless of the season. .

Table 3. Correlation Matrix for CDOM absorption at 440 nm, a_{CDOM}, and spectral slope coefficient. **Significant correlations are marked in bold characters** after p-value test (with significance level α = 0.05). .

	Water	*Coniferous Forest*	*Mixed Forest*	*Meadow*	*Wetland*	*Agriculture*
S_{CDOM}	-0.744	0.585	0.387	**0.984**	**0.916**	**-0.980**
a_{CDOM}	-0.510	0.421	0.166	0.882	**0.933**	**-0.944**
	Urban	***Pasture***	***Discharge***	***Dev****	***Natural****	***Ratio****
S_{CDOM}	-0.878	-0.767	0.829	**-0.985**	**0.998**	**-0.975**
a_{CDOM}	**-0.980**	-0.648	0.815	**-0.964**	**0.931**	**-0.926**

Overall, the CDOM absorption, a_{CDOM}, decreases with increasing proportion of developed areas, although this trend also depends on the time of year. **Figures 9a** shows the trend for spring, while **Figure 9b** shows the trend for summer (each based on the average values per bay and per season). The slope of CDOM, S_{CDOM} (Figure 8b) shows a similar spatial trend as a_{CDOM}, apart from in Hfj. The overall decreasing trend indicates that more natural LULC types will generate more humic acids, whereas the more developed bays (Himmerfjärden and Bråviken) tend to have a lower spectral slope factor, and thus contain a higher proportion of fulvic acids. Note the very large variability of the S_{CDOM} in Himmerfjärden bay. Seasonal variability can be here rejected as explanation as the highest value (Aug-2010) and the lowest value (Aug-2017) were both obtained during measurement campaigns in summer. The large variability in Himmerfjärden bay is likely to be due to the influence of Himmerfjärden Sewage Treatment Plant situated in the inner bay, where nitrate is treated by bacterial breakdown **[33]**. Besides breaking down nitrates, the bacteria may also use CDOM as a substrate, and break down the larger humic acids to fulvic acids. On the other hand during periods of flooding, untreated stormwater may enter the bay, and thus giving rise to larger humic acids.

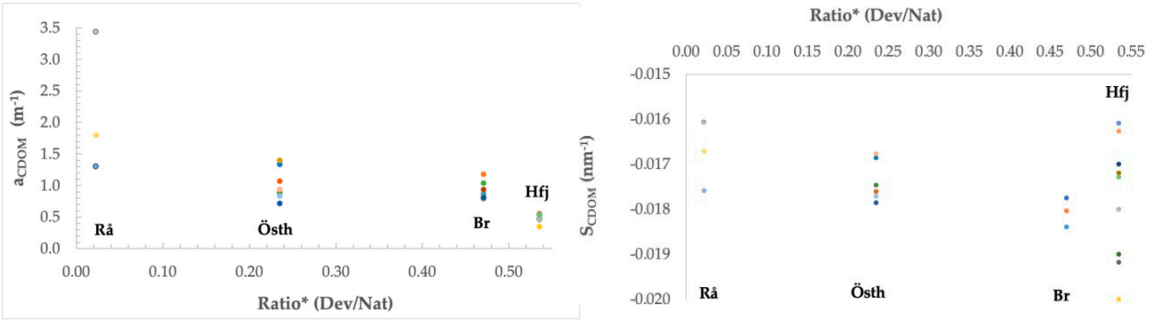

(a) (b)

Figure 8. a. CDOM Absorption at 440 nm, aCDOM, against the LULC category Ratio* (Dev/Nat); all transects for all seasons. **Figure 8b.** Averaged slope factor per transects against the ratio of developed to natural areas: *Ratio** (Dev/Nat) per bay; Råneå (Rå), Östhammar (Östh), Bråviken (Br) and Himmerfjärden (Hfj) - all transects for all seasons. .

Preprints (www.preprints.org) | NOT PEER-REVIEWED | Posted: 20 September 2023 doi:10.20944/preprints202309.1382.v1

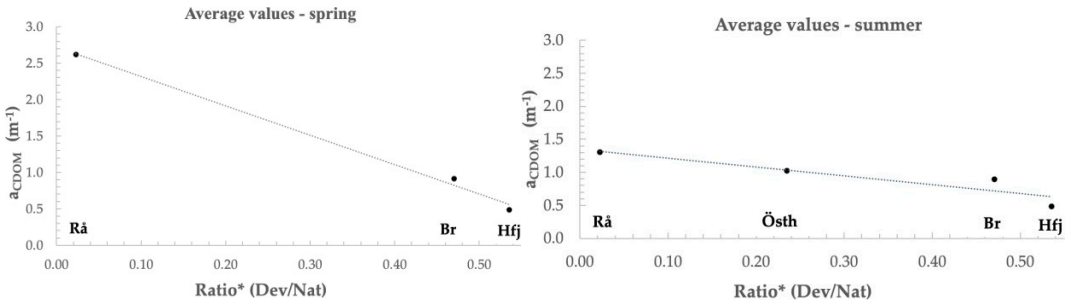

(a) (b)

Figure 9. a. CDOM Absorption at 440 nm, a_{CDOM}, against the LULC category *Ratio** (Dev/Nat) average value per transect and bay in summer, and **9b.** average value per transect and bay in spring; Råneå (Rå), Östhammar (Östh), Bråviken (Br) and Himmerfjärden (Hfj). Note the difference in slope between Figure 9a and 9b. .

3.2. Investigating the nature of particulate material with LULC

Overall, the Suspended Particulate Matter (SPM) and turbidity correlation analyses did not show such clear trends as CDOM absorption and slope across the different areas of interest, apart from Suspended Particulate Inorganic Matter, SPOM (Table 4) which showed a positive significant relationship with the LULC classes *Coniferous Forest*, *Mixed Forest* and *Meadow*, and thus with the *Natural** classes, while it showed a negative relationship with *Agriculture*, and the ratio of developed to natural classes *(Ratio*).*

Table 4. Correlation Matrix for SPM, SPOM and turbidity. Significant correlations are highlighted in bold characters after p-value test (with significance level $\alpha = 0.05$).

	Water	*Coniferous Forest*	*Mixed Forest*	*Meadow*	*Wetland*	*Agriculture*
SPM	-0.274	0.739	0.588	0.538	**-0.991**	-0.895
SPOM	-0.848	**0.999**	**0.979**	**0.964**	-0.824	**-0.963**
Turbidity	0.164	0.379	0.185	0.125	-0.839	0.618
	Urban	***Pasture***	***Discharge***	***Natural****	***Dev****	***Ratio****
SPM	-0.884	0.714	**-0.978**	0.646	-0.925	0.866
SPOM	-0.344	0.060	- 0.586	**0.991**	-0.941	**-0.978**
Turbidity	**-0.999**	0.945	**- 0.973**	0.256	-0.672	0.672

3.3. Investigating the dependency of the Chl-a concentration on LULC

Figure 10 displays the average Chl-*a* values for a given field campaign plotted against the ratio of *Developed* to *Natural (Dev/Nat)* LULC. Råneå bay clearly stands out with its relatively low Chlorophyll-a concentrations, both in spring and summer. This is likely to be related to the high CDOM absorption with very large values found in coastal areas of the Bothnian bay (Figure 7a). Indeed, the strong light attenuation by CDOM in this area has been shown to limit the growth of phytoplankton and algae, and instead to favour bacterial production **[23].** Since the Råneå measurements clearly stand out when compared to the other bays, it has been rejected from the correlation matrix for the remainder of the analysis. The motivation for this is that the relatively low Chl-a levels here are most likely due to light limitation by CDOM rather than caused by different LULC categories. The correlation matrix (table 5) shows significant negative correlations for *Chl-a* with the classes *Agriculture*, *Wetland*, *Developed* as well as the Ratio of *Dev/Nat*.

Preprints (www.preprints.org) | NOT PEER-REVIEWED | Posted: 20 September 2023 doi:10.20944/preprints202309.1382.v1

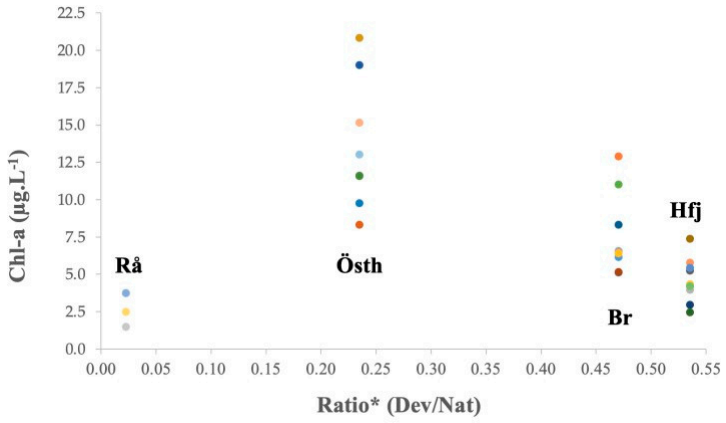

Figure 10. *Chl-a* concentration in four Swedish bays - Råneå (Rå), Östhammar (Östh), Bråviken (BR) .and Himmerfjärden (Hfj) - against ratio of *Developed* to *Natural (Dev/Nat)* LULC.

Table 5. Correlation Matrix for *Chl-a* concentration with LULC categories. **Significant correlations are shown in bold characters** after p-value test (with significance level $\alpha = 0.05$).

.	*Water*	*Coniferous Forest*	*Mixed Forest*	*Heaths*	*Wetland*	*Agriculture*
Chl-a	-0.616	0.938	0.849	0.816	**-0.968**	**-0.997**
	Urban	***Pasture***	***Discharge***	***Natural****	***Dev****	***Ratio****
Chl-a	-0.644	0.398	-0.828	0.886	**-1.000**	**-0.991**

4. Discussion

4.1. LULC classification

The Land Use and Land Cover (LULC) analysis is central in this study, focussing initially on analysing the variation of LULC from one Swedish bay to another. Our LULC classification (Table 2) gave a similar result as the one performed by Franzén et al. **[34]** who classified the sub-catchment area around Himmerfjärden with 57% forest, 33% land, 4% lake and 5% urban areas. We decided to use the great catchment in our study, assuming that the optical properties in the whole catchment are carried downstream, and therefore influence the optical properties of the bay. Gullstrand *et al.* **[35]** classified Bråviken with 49% forest, 18% agriculture and 20% water which, again is quite similar to our classification (Table 2), even though we decided to include the greater catchment rather than just the surrounding catchment of the bay. As the bays also differ in their surrounding and catchment areas, it is likely that the bio-optical properties are influenced by the variation of the land cover and land use in each area. Table 2 shows that the leading LULC category in each catchment area is the category *Coniferous Forest,* followed by *Mixed Forest*. The dominance of *Coniferous Forest* is very typical for Swedish forests **[32]**. Our LULC analysis also confirms previous work showing that catchments in boreal regions are mostly covered with coniferous and mixed forests **[36]**, carrying high concentrations of terrestrial dissolved organic matter (DOM) downstream during the productive seasons. Additionally, there are usually wetlands and bogs in boreal areas, which have the tendency to hold large quantities of organic matter **[37]**. CDOM usually increases in spring after the ice melt, followed by a decrease in summer and an increase, again, during autumn **[5,38]**. Said Al-Kharusi **[39]** proposed that recent advances in remote sensing technology, GIS and modelling could improve our understanding of CDOM in inland waters on large geographic scales. The same has been demonstrated here for the distribution of CDOM in coastal waters.

4.1.1. Influence of LULC classification on a_{CDOM} and S_{CDOM}.

 doi:10.20944/preprints202309.1382.v1

As shown in the results section, $\mathbf{a}_{CDOM}$ and $\mathbf{S}_{CDOM}$ are both positively related to *Wetland*, and the *Natural** LULC classes while they are negatively correlated to *Agriculture* and the *Developed* classes. Zheng et al. **[40]** found positive correlations for $\mathbf{a}_{CDOM}$ and $\mathbf{S}_{CDOM}$ with the natural categories *Forest* and *Grassland* in the yellow river basin. An explanation why we did not find a significant positive correlation with *Forest* might be that our forests are mostly dominated by coniferous trees. Plant material starts degrading during autumn, and is slowly being broken down to humic substances which accumulates on land and in ice and snow during the winter. During the ice melt in spring, this CDOM of terrigenous source is then drained into coastal waters. The minimum range of CDOM values (around 1 m^{-1}) is found in Himmerfjärden bay (corresponding to the average value in the middle of the transect). Note that **Zone I** does not exhibit any strong peaks in discharge for the thawing in spring, based on the hydrological data from SMHI **[26].**

The results shown in **Figures 9a** and **9b** clearly indicate a seasonal variability in the optical properties. The results show a steeper (decreasing) average slope in spring than in summer. According to the correlation matrix (table 3), *Wetland* and *Meadows* showed significant and positively correlated coefficients with the CDOM slope factor. This means the higher the wetland or meadow percentage area, the greater the slope factor, and thus the more humic the type of CDOM (i.e. a slope closer to -0.0011), Carder et al. **[4].**

We also find that the categories *Agriculture, Developed* and also *Ratio** each show a significant, negative correlation with S_{CDOM}. The influence of developed categories is more difficult to interpret. One explanation could simply be the degradation of CDOM, either by UV light (a phenomenon called photobleaching, or fading) and degradation by bacteria. Indeed, CDOM is naturally broken down progressively - chemically or physically – in these ways. For instance, Hulatt et al. **[41]** found that photo bleaching can cause a significant increase in the spectral slope factor (by 0.004 nm^{-1}), that is to say that CDOM tends to get progressively more broken down into smaller fractions, and thus tends to get a more fulvic profile (i.e. a slope closer to -0.0022). Therefore, Agriculture and other developed categories might influence the CDOM slope factor by enhancing the decomposition of CDOM. Williams et al. **[4]** found that dissolved organic matter (DOM) in streams influenced by agriculture was more labile and more accessible to microbial degradation than DOM found in wetland streams, supporting lower rates of microbial activity. Such result suggests that the *Developed** classes of LULC will be likely to stimulate bacterial breakdown of CDOM, and thus be more likely to generate a higher content of smaller fulvic acids.

4.1.2. Influence of LULC classification on SPM

As mentioned before, there were no obvious relationships between total SPM and LULC cover. However, for suspended particulate organic matter (SPOM) significant and robust relationships were found for the classes *Coniferous* and *Mixed Forest*s, as well as *Meadows* and the categories *Natural** and *Ratio** (see table 4) while the *Agricultural* class showed a negative but significant correlation. One could explain the positive correlations with predominantly natural categories by the fact that they generate a lot of pollen in spring and summer. Pollen constitutes indeed an important fraction of SPM in natural waters **[43]** and in the Baltic Sea **[44].** Viennet **[43]** focused his study on morpho-granulometry analysis as to investigate the nature, origin and transfer of SPM. He found that SPM consists of three main categories: mineral particles (silica sands and clays), organic matter (coal, carbonized OM), peat and loam (humus-containing soil) and other biologic matter (phytoplankton and pollen). This may therefore explain the occurrence of strong relationships between SPOM on the one hand, and forests on the other hand. Pawlik and Ficek **[44]** found that in many areas of the central Baltic Sea, pine pollen can constitute up to 50% of the SPM in the 1.25-250 μm size range during spring.

Agriculture was found to be negatively correlated with SPOM (but not with SPIM) and agricultural land thus seems to act as sink of organic matter. Wetland showed a significant negative correlation with total SPM. Such a result was also found by Le et al. **[19]** and is coherent with the hypothesis that bogs may act as sinks for suspended material which may fall out and settle. Furthermore, plants and their roots may act as physical barriers preventing erosion, and thus also

decreasing the SPM concentration. Some of the findings regarding SPM are contradictory to the literature. For example, one may hypothesise that the inorganic fraction (SPIM) would be positively correlated with the *Urban* and *Agriculture* classes as shown in Le et al. **[19]** in the Gulf of Mexico. This relies on the assumption that developed areas give rise to more exposed soils or barren land, allowing for more runoff of sediments and other particulates into rivers and, eventually the sea. However, considering SPM and SPIM, we did not find any significant relationships to any of the investigated LULC types. This may partially be due to the fact that the *Urban* class only made up a very small percentage in each area of interest (ranging from 0.3 % to 4.4 %), which is rather low compared to the main categories. Also, given that our study is in a completely different vegetation zone, the results from the study by Le et al. **[19]** in the Gulf of Mexico, with very large and continued high run-off and larger *Urban* proportions as well as a lack of seasonal influence, cannot be simply assumed to also apply to high latitudes.

It must also be noted, that the bays in zone I all had a relatively low discharge over the year, while Råneå showed a very strong discharge in spring (Supplementary Figures S3a-3c), while its urban category is negligible (0.3 %). This means that the nature of our data set does not allow to properly investigate the effect of the *Urban* class.

4.1.3. Influence of LULC classification on Chl-a

We found a non-significant negative relationship with C*hl-a* concentration for the *Urban* class (Table 5) which may be related to the generally small surface areas of the urban classes in our catchment areas. The negative correlation between *Wetland* and *Chl-a* indicate that *Wetland* acts as a sink. Wetlands are often used as a measure to mitigate the effects of eutrophication. For example, some vegetation types are used as buffer zones around the Baltic Sea coasts in order to fix carbon (and nutrients), and thus reduce nutrient leakage into the Baltic Sea, e.g. wetlands and reed belts. Reed has the potential to sequester nutrients and to stabilize soils, as well as to reduce heavy metals **[45].** By growing reed one can therefore reduce erosion and drainage of SPM, and at the same time reduce the 624 drainage of nutrients if the reeds are harvested, and for example used as cow feed. Furthermore, underwater seagrass meadows can also act as nutrient and sediment traps **[46]** and are therefore also important for the reduction of *Chl-a* and SPM contents in coastal bays.

5. Conclusions

This macroscopic study of four Swedish bays with their respective catchments lead to some compelling findings. Land Use and Cover analysis allows to investigate the nature of CDOM in the Baltic Sea. For instance, with a GIS analysis assessing the percentage of land cover one can then approximate the slope value of CDOM, S_{CDOM} : around -0.019 for *Natural/Wetland* covered watershed; around -0.015 in more developed catchments. Given that only limited information exists regarding the specific IOPs such as S_{CDOM} in Swedish coastal areas, CDOM estimates based on LULC classification may show to be useful in the local or regional adaptation of bio-optical and/or remote sensing algorithms. This study shows that the CDOM absorption mean value for a given bay can also be approximated by mapping the extent of *Natural* land cover (*Wetland* and *Meadow*). Moreover, the strong correlation found between SPOM and *Meadow, Mixed Forest* and *Coniferous Forest* seems to indicate that SPOM mostly originates from pollen. Furthermore, this study also confirms the role of *Wetlands*, which seem to be a primary terrigenous source of CDOM with high humic character and also physical barriers for SPM, acting as buffer zones and trapping sediments. The correlation analysis for Chl-a showed different patterns and were usually opposite to the findings in Le et al. **[19]**, indicating that complex biological factors may rule Chl-a production, and that these results do not generally apply to ecosystems across different vegetation zones (warm-temperate to subtropical vs. boreal) and may also strongly depend on the nature of dominant LULC categories. Suspended particulate matter and turbidity were the least conclusive parts of this study and require a consideration of other parameters related to physical forcing (e.g. bottom depth of lakes and bays, wind speed and weather condition for a given transect) which was beyond the scope of the study. In further studies, one could also weigh each watershed by its average

discharge value, and thereby account for the relative contribution of each area to the total discharge, and also relate it to the volume of the respective bay.

Supplementary Materials: The following supporting information can be downloaded at the website of this paper posted on Preprints.org, Figure S1: Swedish standing volume by Swedish tree species in percent; Figure S2a-c: Landcover maps for Bråviken, Östhammar and Råneå bays; **S3a-b:** Freshwater discharge value per catchment for the Himmerfjärden, Östhammar (a), Bråviken and Råneå bays (b). Table S1:Corine Land Cover Classes; Table S2: Bio-optical dataset used in this study.

Author Contributions: Conceptualization, SK and MA.; methodology, MA and SK; software, MA.; validation, MA and SK; formal analysis, MA; investigation, MA and SK; resources, SK and MA; data curation, MA; writing—original draft preparation, MA and SK; writing—review and editing, SK; visualization, MA and SK; supervision, SK; project administration, SK.; funding acquisition, SK. All authors have read and agreed to the published version of the manuscript.

Funding: S.K. was funded by the Swedish National Space Agency (SNSA), grant number 2021-00064 and by the Swedish Agency for Marine and Water Management (SwAM), Project No. 538-21. M.A. was funded by the EU ERASMUS^{+} program and by the BRMIE grant of the Auvergne-Rhone-Alpes Region, France.

Data Availability Statement: The bio-optical data set used in this study is available under supplementary material (Supplementary Table S2).

Acknowledgments: The authors would like to thank the pelagic monitoring groups from Stockholm University and Umeå University (UMF) for provision of data and support during field work (UMF). Lots of thanks to Sean o'Kane (Maynooth University, Ireland) and Tom Verheyde (INSA, Lyon, France) for advise on the GIS tools and analysis. Thanks to Prof. Steve Lyon (Ohio State University, USA) for advise on hydrological analysis, and thanks to Dr Jakob Walve (DEEP, Stockholm University) for providing useful feed-back to the manuscript.

Conflicts of Interest: The authors declare no conflict of interest.

References

1. Kirk, J.T.O. *Light and Photosynthesis in Aquatic Ecosystems* (3rd ed.), Publisher: Cambridge University Press, Cambridge, 2010, 639 pp, ISBN: 978-0-521-15175-7.
2. Schnitzer, M. Humic substances: chemistry and reactions. In: *Developments in soil science*. Vol 8: Soil organic matter. M. Schnitzer; S.U. Khan, Eds, Publisher: Elsevier, Amsterdam, The Netherlands, 1978, pp. 1-64.
3. Preisendorfer, R.W. Application of radiative transfer theory to light measurement in the sea. Union of Geodetic Geophysical Institute Monograph, 1961, *10*, 11-30.
4. Carder, K.L.; Steward, R.G.; Harvey; G.R.; Ortner, P.B. Marine humic and fulvic acids: Their effects on remote sensing of ocean chlorophyll. *LIMNOL OCEANOGR* 1989, *34*, 68–81, doi:10.4319/lo.1989.34.1.0068.
5. Harvey, T.; Allart, S.; Andersson, A.; Relationships between Coloured Dissolved Organic Matter (CDOM) and Dissolved Organic Carbon (DOC) in different coastal gradients of the Baltic Sea. *AMBIO* 2015, *44* (3), 392-401, doi:10.1007/s13280-015-0658-4.
6. Kowalczuk, P.; Stedmon, C.A.; Markager, S. Modeling absorption by CDOM in the Baltic Sea from season, salinity and chlorophyll. *MAR CHEM* 2006, *101*(1-2), 1-11. doi.org/10.1016/j.marchem.2005.12.005.
7. Kratzer, S.; Tett, P. Using bio-optics to investigate the extent of coastal waters a Swedish case study, HYDROBIOLOGIA 2009, 629, 169-186, doi:10.1007/s10750-009-9769-x.
8. Robinson I.S. Satellite observations of ocean colour Philosophical Transactions of the Royal Society of London. Series A, Mathematical and Physical Sciences 1983, *309*, 415–432, doi:10.1098/rsta.1983.0052
9. Wild-Allen, K.; Lane, A.; Tett, P. Phytoplankton, sediment and optical observations in Netherlands coastal water in spring. *J SEA RES* 2002, 47(3-4), pp.303-315, doi:10.1016/S1385-1101(02)00121-1.
10. Hulst, H.C., van de. *Light scattering by small particles*, 1981, Publisher: Dover Publications, Inc., New York, 470 pp., ISBN:0-486-64228-3.
11. Carder, K.L.; Betzer, P.R.; Eggimann, D.W. Physical, chemical, and optical measures of suspended-particle concentrations: their intercomparison and application to the West African Shelf. In: *Suspended solids in water*, Gibbs, R.J., Ed.,Publisher: Springer, Boston, MA, 1974, pp. 173-1; doi:10.1007/978-1-4684-8529-5_11.
12. Aas, E. Refractive index of phytoplankton derived from its metabolite composition. *J PLANKTON RES* 1996, *18(*12), 2223-2249, doi:10.1007/978-1-4684-8529-5_11.
13. Lide, D.R. *Physical and optical properties of minerals*. CRC Handbook of Chemistry and Physics, 77th edition, 1996, Publisher: CRC Press, Taylor & Francis, Boca Raton, Florida, USA, p.2608, ISBN-10 0849305969.
14. Boss, E.; Pegau, W.S.; Lee, M.; Twardowski, M.; Shybanov, E.; Korotaev, G.; Baratange, F., Particulate

backscattering ratio at LEO 15 and its use to study particle composition and distribution. *J GEOPHYS RES: OCEANS* 2004, *109*(C1), doi:10.1029/2002JC001514.

15. Kratzer, S.; Kyryliuk, D.; Brockmann, C. Inorganic suspended matter as an indicator of terrestrial influence in Baltic Sea coastal areas—Algorithm development and validation, and ecological relevance. *REMOTE SENS ENVIRON* 2020, *237*, 111609, doi:10.1016/j.rse.2019.111609.
16. Kari, E.; Kratzer S.; Beltrán-Abaunza, J.M.; Harvey, E.T.; Vaičiūtė, D. Retrieval of suspended particulate matter from turbidity–model development, validation, and application to MERIS data over the Baltic Sea. *INT J REMOTE SENS* 2017, *38*(7), 1983-2003, doi:10.1080/01431161.2016.1230289.
17. Miller, R. L.; McKee, B.A. Using MODIS Terra 250 M Imagery to Map Concentrations of Total Suspended Matter in Coastal Waters. *REMOTE SENS ENVIRON* 2004, *93*(1–2), 259–266, doi:10.1016/j.rse.2004.07.012.
18. Kratzer, S.;Moore, G., Inherent Optical Properties of the Baltic Sea in Comparison to Other Seas and OcKratzereans. REMOTE SENS 2018, 10(3), 418, doi:10.3390/rs10030418.
19. Le, C.; Lehrter, J.C.; Hu, C.; Schaeffer, B.; MacIntyre, H.; Hagy, J.D.; Beddick, D.L. Relation between inherent optical properties and land use and land cover across Gulf Coast estuaries. *LIMNOL OCEANOGR* 2015, *60*(3), 920-933, doi:10.1002/lno.10065.
20. HELCOM Sub-basins 2018. Available online: http://metadata.helcom.fi (accessed on 15 August 2022).
21. Natural Earth, Free vector and raster map data Available online: https://www.naturalearthdata.com (accessed on 11 Sept 2022).
22. European Environment Agency, EEA, European Shapefile, Available online: https://www.eea.europa.eu (accessed on 11 Sept 2023).
23. SMHI, 2021, SVAR (Svenskt VattenARkiv) Available online: https://www.smhi.se/data/hydrologi/sjoar-och-vattendrag/ladda- ner-data-fran-svenskt-vattenarkiv-1.20127 (accessed on 11 September 2023).
24. Pekel, J.F.; Cottam, A.; Gorelick, N.; Belward, A.S. High-resolution mapping of global surface water and its long-term changes. *NATURE* 2016, *540*(7633), 418-422, doi: 10.1038/nature20584.
25. SMHI, Hydrologiskt Nuläge, Vattenwebb (in English: Current Hydrological Status, Water Web), Available online: https://vattenwebb.smhi.se/hydronu/ (accessed on 11 September 2023).
26. Andersson, A.; Brugel, S.; Paczkowska, J.; Rowe, O.F.; Figueroa, D.; Kratzer, S.; Legrand, C. Influence of allochthonous dissolved organic matter on pelagic basal production in a northerly estuary. *ESTUAR COAST SHELF S* 2018, *204*, 225-235, doi:10.1016/j.ecss.2018.02.032.
27. Kratzer, S.; Harvey, E.T.; Canuti, E. International Intercomparison of In Situ Chlorophyll-a Measurements for Data Quality Assurance of the Swedish Monitoring Program. *FRONT. REM SENS* 2022, *3*, p.866712, doi:10.3389/frsen.2022.866712.
28. Strickland, J.H.D.; Parsons, T.R., *A practical hand-book of sea-water analysis*. Bulletin Journal of the Fisheries Research Board of Canada, Pergamon Press, Oxford, England, 1972, *167*, p. 185–203, ISBN0-08-030-288-2.
29. Kratzer, S. Bio-optical Studies of Coastal Waters. PhD thesis; monograph in English. School of Ocean Sciences, University of Wales, Bangor (UWB), UK, 2000, ISNI 0000 0001 3602 4205.
30. Parsons, T. R.; Maita, Y.; Lalli, C. M. *A Manual of Chemical and Biological Methods for Seawater Analysis*, Pergamon Press, Oxford, England, 1984, 173 pp, ISBN 0-08-030288-2
31. Sørensen, K.; Grung, M; Röttgers, R. An intercomparison of in vitro chlorophyll a determinations for MERIS level 2 data validation. *INT J REMOTE SENS* 2007, *28* (3-4), 537-554, doi:10.1080/01431160600815533.
32. SLU, *Official statistics of Sweden*. Swedish University of Agricultural Sciences, Umeå, Sweden, Publikationsservice, Uppsala, 2017, ISSN 0280-0543.
33. Cema, G.; Płaza, E.; Trela, J.; Surmacz-Górska, J. Dissolved oxygen as a factor influencing nitrogen removal rates in a one-stage system with partial nitritation and Anammox process. *WATER SCI TECHNOL* 2011, *64*(5), pp.1009-1015, doi:10.2166/wst.2011.449.
34. Franzén, F.; Kinell, G.;Walve, J.; Elmgren, R.; Söderqvist, T. Participatory social-ecological modeling in eutrophication management: the case of Himmerfjärden, Sweden. *ECOL SOC* 2011, *16*(4), 27. Doi:10.5751/ES-04394-160427.
35. Gullstrand, M.; Löwgren, M.; Castensson, R. Water issues in comprehensive municipal planning: a review of the Motala River Basin. *J ENVIRON MANAGE* 2003, 69(3), 239-247, doi:10.1016/j.jenvman.2003.09.007.
36. Laudon H.; Berggren M.; Ågren A.; Buffam I.; Bishop K.; Grabs T.; Jansson M.; Köhler, S. Patterns and dynamics of Dissolved Organic Carbon (DOC) in boreal streams: the role of processes, connectivity, and scaling. *ECOSYSTEMS* 2011, *14*, 880-93.

doi:10.1007/s10021-011-9452-8.

37. Mzobe, P.; Berggren, M.; Pilesjö, P.; Lundin, E.; Olefeldt, D.; Roulet, N.T.; Persson, A. Dissolved organic carbon in streams within a subarctic catchment analysed using a GIS/remote sensing approach. *PLOS ONE* 2018, *13*(7), p.e0199608, doi:10.1371/journal.pone.0199608.

38. Ågren, A.; Buffam, I.; Berggren, M.; Bishop, K.; Jansson, M.; Laudon, H. Dissolved organic carbon characteristics in boreal streams in a forest-wetland gradient during the transition between winter and summer. *J GEOPHYS RES-BIOGEO* 2008, *113*(G3), doi:10.1029/2007JG000674.
39. Said Al-Kharusi, E. Broad-Scale Patterns in CDOM and Total Organic Matter Concentrations of Inland Waters – Insights from Remote Sensing and GIS. PhD thesis, Dept of Physical Geography and Ecosystem Science, Faculty of Science, Lund University, Sweden, 2021, ISBN (electronic) 978-91-89187-04-7.
40. Zheng, K.; Shao, T.; Ning, J.; Zhuang, D.; Liang, X. Water quality, basin characteristics, and discharge greatly affect CDOM in highly turbid rivers in the Yellow River Basin, China. *J CLEAN PROD* 2023, *4*, 136995, doi:10.1016/j.jclepro.2023.136995.
41. Hulatt, C.J.,;Thomas, D.N.; Bowers, D.G.; Norman, L.; Zhang, C. Exudation and decomposition of chromophoric dissolved organic matter (CDOM) from some temperate macroalgae. *ESTUAR COAST SHELF S* 2009, *84*(1), 147-153, doi:10.1016/j.ecss.2009.06.014.
42. Williams, C.J.; Yamashita, Y.; Wilson, H.F.; Jaffé, R.; Xenopoulos, M.A., Unraveling the role of land use and microbial activity in shaping dissolved organic matter characteristics in stream ecosystems. *LIMNOL OCEANOGR* 2010, *55*(3), 1159-1171, doi:10.4319/lo.2010.55.3.1159.
43. Viennet, D. The use of morphogranulometry in source to sink monitoring of particle transfer in watersheds. PhD dissertation, École doctorale Normande de biologie intégrative, santé, environnement, Mont-Saint-Aignan, Seine-Maritime, France, 2020, viaf.org/viaf/408160483843904992099.
44. Pawlik, M.M.; Ficek, D. Spatial Distribution of Pine Pollen Grains Concentrations as a Source of Biologically Active Substances in Surface Waters of the Southern Baltic Sea. *WATER- SUI* 2023, *15*(5), 978, doi:10.3390/w15050978.
45. Karstens, S.; Buczko, U.; Jurasinski, G.; Peticzka, R.; Glatzel, S., Impact of adjacent land use on coastal wetland sediments. *SCI TOTAL ENVIRON* 2016, *550*, 337-348, 2016, doi:10.1016/j.scitotenv.2016.01.079.
46. Dahl, M.; Asplund, M.E., Björk, M.; Deyanova, D.; Infantes, E.; Isaeus, M.; Nyström Sandman, A.; Gullström, M. The influence of hydrodynamic exposure on carbon storage and nutrient retention in eelgrass (*Zostera marina* L.) meadows on the Swedish Skagerrak coast. *SCI REP-UK* 2020, *10*(1), 1-13, doi:10.1038/s41598-020-70403-5.